Quantum dot microcavity control of photon statistics

Snijders, H.J.

Chapter 1

Introduction

In this thesis, we study the photon statistics of light emitted by a microcavity that contains a single quantum dot (QD) on resonance. The light is described in terms of photon Fock states, and the excitonic transitions in a QD can be considered as a two-level system. The transition from one QD state to the other happens by absorption or emission of a photon. We now consider such a two-level system which is resonantly interacting with light that is focused to a beam waist ω_0. Deterministic interaction between the two-level system and the photon requires that the absorption cross section $\sigma_{abs} = \frac{3\lambda^2}{2\pi}$ of the two-level system is much larger than the area of the light beam $A = \pi\omega_0^2$. Here, λ is the wavelength of the light. This condition ($\sigma_{abs} \gg A$) is not achieved in free space but can be achieved in a cavity [1]. This can be done with a Fabry-Perot cavity with two mirrors with reflectivity R. A photon bounces back and forth many times between these mirrors and the number of bounces is characterized by the finesse $\mathcal{F} = \frac{\pi\sqrt{R}}{1-R}$. In the case of a high finesse cavity it becomes possible to satisfy the condition

$$\sigma_{abs} \gg A \quad \rightarrow \quad \frac{3\lambda^2}{2\pi} \times \frac{\mathcal{F}}{\pi} \gg \pi\omega_0^2. \tag{1.1}$$

This enables deterministic interaction between a photon and a single QD and leads to intriguing quantum effects. In this thesis, we study this interaction in a solid-state system and show how the photon statistics can be tuned from anti-bunching, leading to high quality single-photon sources [2, 3, 4], to strongly bunched [5].

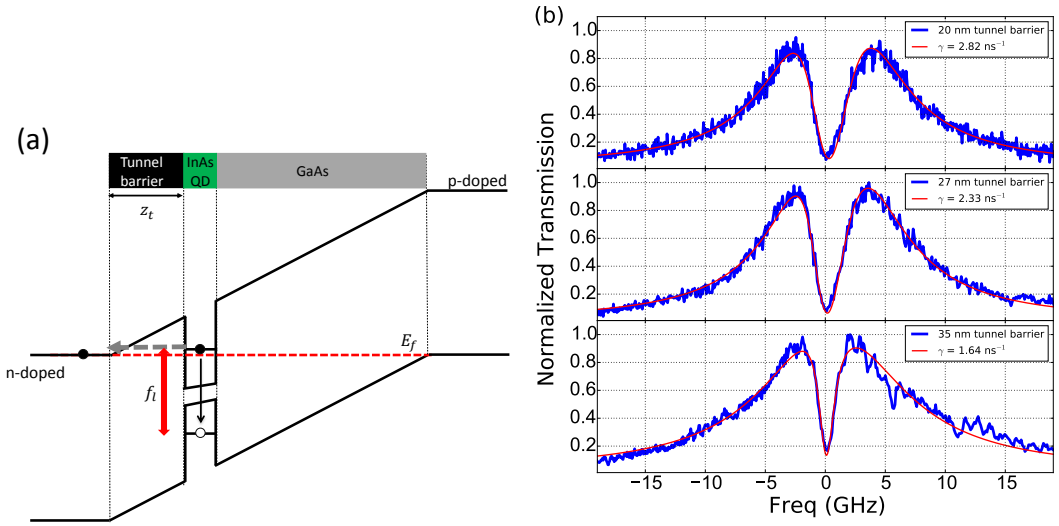

Figure 1.1: a) Sketch of the band structure of the p-i-n region in a micropillar cavity. b) Cavity transmission with on-resonance an exciton transition as a function of the laser frequency. Three plots for different tunnel barrier thicknesses are shown.

1.1 A QD in a micropillar cavity

In this part we discuss the structure and properties of a solid-state quantum dot (QD) micropillar device. The QDs we use are self-assembled semiconductor QDs grown in Stranski–Krastanov [6] growth mode using molecular beam epitaxy. On a gallium arsenide (GaAs) buffer we deposit indium and arsenide. At some point due to the lattice mismatch between GaAs and indium arsenide (InAs), it becomes energetically favorable to form small nanometer-scale islands at random positions on the wafer. The height and shape of these islands depend on the temperature and other growth conditions. Afterwards, the indium arsenide (InAs) islands are capped with a gallium arsenide layer. Since the semiconductor band gap of InAs islands is smaller than the band gap of the surrounding GaAs, electronic states within the InAs are similar to the discrete quantum states of a "particle in a box". Together with the selection rules, the QD enables specific discrete optical transitions just like atoms.

We embed the QDs in the active region of a p-i-n device. Figure 1.1(a) shows a sketch of the band structure, where the red dashed line indicates the Fermi level. Only a single transition in the QD is sketched which is resonant with the laser frequency f_l. The bound state between the electron and hole of this transition is called an exciton. Here a "hole" could be seen as a missing electron in a filled energy level. This exciton can be physically interpreted as a dipole, where the electron represents a negative charge and the hole a positive charge.

Recombination of an electron-hole pair is not the only way for an electron to leave a specific energy level. It is also possible for the electron to tunnel out of the QD. This process is indicated by the gray dashed arrow in Fig. 1.1(a). If the tunnel barrier thickness z_l increases, the probability for the electron to tunnel out of the QD decreases.

Below and above the active layer with randomly distributed QDs we grow a Bragg

reflector. A Bragg reflector is formed from multiple layers of alternating materials with varying refractive index, where each layer boundary causes partial reflection of an optical wave. For normal wave incidence the thickness of each optical layer thickness is corresponding to one quarter of the wavelength for which the mirror is designed. For the design wavelength, the optical path length difference between reflections from subsequent interfaces is half the wavelength. Combined with the fact that the amplitude reflection coefficient for the interfaces have alternating signs, constructive interference or strong reflection appears. The distributed Bragg reflectors and active layer are critical components in our design and are based on the designs of vertical cavity surface emitting lasers, which are nowadays important ingredients in photonics [7].

A sketch of the device containing a Bragg cavity and a QD layer is given in Fig. 1.2(a), additionally, we also add electronic contacts to the device and an oxide aperture. The electronic contacts allow the device to function as a p-i-n junction, to slightly tune the QD frequency into resonance with the cavity mode. The oxide aperture is for in-plane light confinement: oxidation of an aluminium arsenide layer leads to formation of aluminium oxide and a reduction of the refractive index from $n \approx 3$ to $n \approx 1.5$ [8], so that the light is confined in the central unoxidized region. Compared to more commonly used air-guided micropillars [9], our design has advantages: higher mechanical stability, and the ability to easily electrically contact the micropillar.

We use a tunable narrow linewidth laser to measure the transmission from the micropillar cavity as a function of laser frequency. For an empty cavity we observe a Lorentzian line shape in transmission, while in the presence of a QD in the cavity, a dip appears in the transmission spectrum at the QD resonance (see Fig. 1.1(b)). In Fig. 1.1(b) we show that, for increasing tunnel barrier thickness (20, 27, and 35 nm), the linewidth of the dip in the cavity transmission spectrum reduces. This example shows the complexity and challenges in making a QD micropillar cavity: varying the thickness of the tunnel barrier by only a couple of nanometers leads to significant changes in the transmission spectrum.

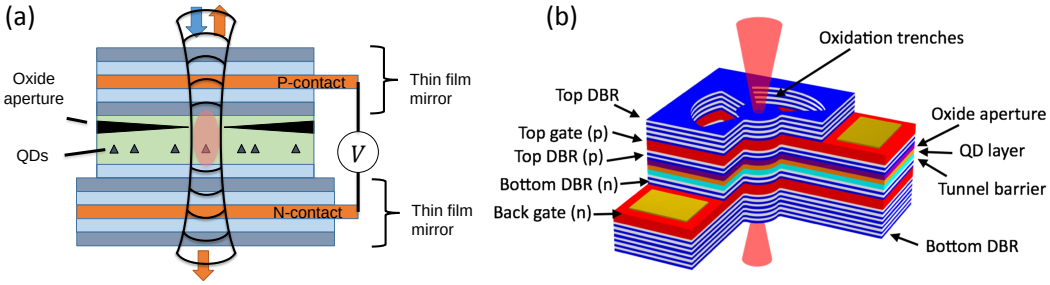

Figure 1.2: a) Cross-sectional sketch of our micropillar device, where we indicate the Bragg mirror (DBR), QDs, oxide aperture and contacts. b) Three dimensional sketch, showing the trenches used for oxidation and aperture formation.

1.2 Optical characteristics of a QD in a micropillar cavity

In Fig. 1.3(a) we show a false color plot of the typical transmission through the micropillar as a function of the laser frequency and the voltage applied over the structure. By varying the voltage we change the slope of the bands in Fig. 1.1(a), which shifts the position of

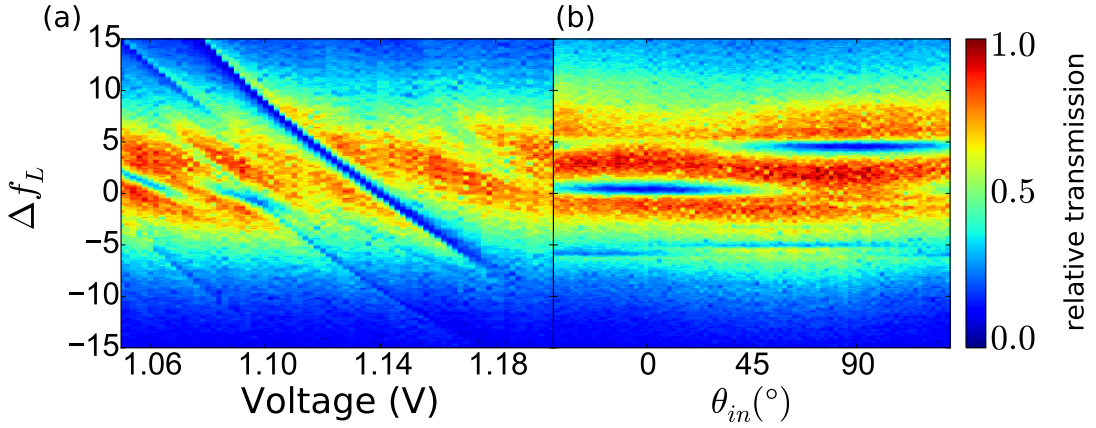

Figure 1.3: a) The cavity transmission of linearly polarized light ($\theta_{in} = 0°$) as a function of the laser frequency f_l and the voltage applied over the device. b) Similar false color plot of the cavity transmission but now as a function of the linear input polarization at a fixed voltage of 1.14 V. In both cases the transmission is measured without any filters or an output polarizer.

the QD with respect to the Fermi level, and the transition energy. In Fig. 1.3(a) there are multiple QDs present but there is only one QD where the exciton transition is coupled strongly to the cavity. For this QD we observe that, if on-resonance, the transmission properties of the cavity are severely changed. A dip appears in the spectrum and most of the light is no longer transmitted. Throughout this thesis the measurements are typically carried out in transmission, but could also be performed in reflection.

Due to fabrication and material imperfections, the circular symmetry of the micropillar cavity is broken. This results in two orthogonal linearly polarized cavity modes. The shape and birefringence of the cavity determines the resonance frequency of each cavity mode. At 1.14 V we measure in Fig. 1.3(b), for a nearly polarization degenerate cavity, the transmission as a function of the input polarization and frequency of the light. Next to the polarization dependence of the cavity modes, we observe here that the QD has two linearly polarization transitions, this is due to the exciton fine-structure splitting. The two orthogonally polarized transitions appear with a slight difference in energy, which only disappears if the QD is rotational symmetric. In Fig. 1.3(b) these polarization axes are at 0° and 90° and are split several GHz apart. In section 2.4, we present a theoretical semi-classical model incorporating the polarization features of the cavity and QD. Typically, the polarization axes of the QD dipole and the cavity are not aligned with respect to one another and this misalignment opens up another possibility for the device to function as a single-photon source, as will be discussed in chapters 2 and 7.

1.3 Theoretical description of light-matter interaction

The interaction between a light field and a two-level system can be modeled as a dipole in an electric field. The Hamiltonian for this interaction is [10]

$$H_I = \hat{\boldsymbol{d}} \cdot \hat{\boldsymbol{E}}, \tag{1.2}$$

where $\hat{\boldsymbol{d}}$ is the dipole moment operator and $\hat{\boldsymbol{E}}$ is the electric field operator of a single cavity mode. Quantizing the electric field without the time-dependence $e^{i\omega t}$ leads to

$$H_I = \hat{\boldsymbol{d}} \cdot \boldsymbol{e} E_0 \left(\hat{a} + \hat{a}^\dagger \right), \tag{1.3}$$

with $E_0 = -\left(\frac{\hbar\omega}{\epsilon_0 V}\right)^{1/2} \sin(kz)$. Here, ω is the frequency of the mode and k is the wave number related by $k = \omega/c$. z is the axial coordinate and V is the effective volume of the cavity. $\boldsymbol{e}$ is the cavity mode polarization vector. The dipole operator facilitates an atomic transition from the ground state to the excited state or vice versa by

$$\hat{\boldsymbol{d}} \cdot \boldsymbol{e} = d \left|g\right\rangle \left\langle e\right| + d^* \left|e\right\rangle \left\langle g\right| \equiv \frac{2d}{\hbar} \left(\hat{S}_- + \hat{S}_+ \right), \tag{1.4}$$

where we assume that the constant d is real, $|g\rangle$ is the ground state and $|e\rangle$ is the excited state of the two-level system. This leads to the interaction Hamiltonian

$$H_I = \frac{2dE_0}{\hbar} \left(\hat{S}_- + \hat{S}_+ \right) \left(\hat{a} + \hat{a}^\dagger \right). \tag{1.5}$$

In the rotating wave approximation, we obtain what is widely known as the Jaynes–Cummings interaction Hamiltonian

$$H = g \left(\hat{S}_+ \hat{a} + \hat{S}_- \hat{a}^\dagger \right), \tag{1.6}$$

where $g = \frac{2dE_0}{\hbar}$. The Jaynes–Cummings Hamiltonian is one of the main mathematical tools that connect light and matter on a fundamental level and in Chapter 2 we will discuss it in much more detail.

1.4 Applications of light-matter interactions

From an application point of view, there are several reasons to study light-matter interaction. For example, it plays a crucial role in quantum networks [11], where quantum information is transferred between quantum nodes. One of the main advantages of quantum networks over classical networks is security [12, 13]. The basis for this lies in the axiom that one cannot in general take a measurement on a quantum system without perturbing the system. This means that if we have a communication channel between A and B, then a malicious eavesdropper cannot get any information about the communication without introducing perturbations that would reveal its presence. This means that, theoretically, we can make a guaranteed, by the laws of quantum physics, secure communication channel. To create a quantum network over long distances, one needs a system that suffers minimally from decoherence. Photons [14] are a viable option to distribute quantum information since they have only limited interaction in free space. They also benefit from a range of degrees of freedom (such as polarization) which can encode quantum information. However, the very property that makes photons ideal for transporting quantum information, makes it also hard to initially transfer the quantum information onto the photons. In order to solve that problem we need devices that have efficient light-matter interaction to function as a node in a quantum network. Another application is to replace electrons with photons in on-chip and inter-chip interconnects,

which could significantly reduce the energy consumption in large data centers because of the lower Ohmic loss or heat production.

In this thesis, however, the focus is more on the fundamental physical properties of light-matter interaction. The work is centered around experiments that manipulate photon statistics and we analyze the results using classical, semi-classical and quantum models.

1.5 Outline of this thesis

In chapter 2, we give a detailed description of the semi-classical model. It is shown how the model can be solved under certain approximations and we present a method to derive the semi-classical model from fully classical principles. We present an extension of the semi-classical model to a model which incorporates multiple optical transitions and two cavity modes. Furthermore, we show how this model can be used to improve the efficiency of a single-photon source.

In chapter 3, the full quantum master equation is solved and compared to results obtained in chapter 2. This gives us an indication for the parameters in which regime the semi-classical model is sufficient for describing the experimental results. In the final section of this chapter, we discuss how to formulate a quantum master equation for different types of level structures, corresponding to the exciton, biexciton and trion. It shows the complications one needs to take into account when studying light-matter interaction for systems with more involved level structures. Furthermore we argue why the quantum master equation is a useful tool.

In Chapter 4, we discuss the purification of a single photon non-linearity. We show that, for a low mean photon number, extreme photon correlations $\left(g^{(2)}(0) \approx 40\right)$ can be obtained in the weak coupling regime. This is possible because we remove the single-photon component of the light.

In chapter 5, we again tune the photon statistics of light and, instead of filtering the single-photon Fock state from the input light, the two-photon Fock state is removed. An explanation of this effect is given in terms of interference between two excitation pathways to the $N = 2$ photon state, which can be destructive thanks to small energy shift of the two-photon state induced by the weak QD nonlinearity. This alternative mechanism for creating single photons is called the unconventional photon blockade (UPB) and we give here a first experimental demonstration of this effect.

In chapter 6, we describe in detail how the unconventional photon blockade can be described in terms of squeezing and displacement of non-classical Gaussian states of light. Additionally, we describe a method by which this squeezing can potentially be measured.

Chapter 7 discusses the first experimental realization of a resonantly pumped fiber-coupled single-photon source. The characteristics of the device, given by the purity, indistinguishability, and repetition rate of the photons, are state of the art. Together with the fiber coupling, the device becomes usable for commercial applications.